Numerical Simulation of Transonic Separated Flows over Low-Aspect-Ratio Wings

Ünver Kaynak*
Sterling Software, Palo Alto, California
Terry L. Holst†
NASA Ames Research Center, Moffett Field, California
Brian J. Cantwell‡
Stanford University, Stanford, California
and
Reese L. Sorenson§
NASA Ames Research Center, Moffett Field, California

Transonic flowfields about a low-aspect-ratio advanced technology wing have been computed using a viscous/inviscid zonal approach. The flowfield near the wing where viscous effects are important was solved using the "Reynolds-averaged Navier-Stokes equations" in "thin-layer" form. The Euler equations were used to determine the flowfield in regions away from the wing where viscous effects are insignificant. A zonal grid using an H-H topology was generated around the wing by first solving a set of Poisson's equations for the global grid. This grid was then subdivided into separate zones of viscous or inviscid flow as suggested by the flow physics. A series of flow cases were computed and compared with corresponding sets of experimental data. All cases showed good agreement with experiment in terms of the pressure field. Also, an encouraging correlation between computed separated surface flow and experimental oil flow was obtained.

Introduction

LIFTING surfaces such as wings, canards, strakes, etc., play an important role in the design process. Accounting for separated flows around these surfaces is one of the most crucial tasks of aerodynamic design. There are primarily two motivations for understanding separated flows[1]: 1) since uncontrolled separation causes stall, controlling and minimizing its effects are desirable, and 2) separation can also be used to improve aerodynamic performance. For instance, the rolled-up vortex sheet from the sharp leading edge of a delta wing or strake creates so-called "nonlinear lift," which can be intelligently exploited by fighter aircraft designers.

Our present understanding of three-dimensional flows involving separation on wings comes mainly from flow visualization experiments with surface-oil techniques in wind tunnels, smoke tunnels, and dye flow in water tunnels. However, there have also been some attempts to compute separated flows on wings in recent years. Numerical calculations of the leading-edge vortex associated with a delta wing have been made using potential flow procedures[2,3] or Euler equation methods.[4-7] Also, mildly separated flows were computed using viscous-inviscid interaction methods, but they are yet to mature.[8]

On the other hand, the Navier-Stokes equations seem to be needed for accurately computing massively separated flows.[1] Although this approach as it is applied to three-dimensional flow over wings is new, a number of publications are now appearing on the subject. The computation of the supersonic flow over a blunt delta wing by Vigneron et al.,[9] the leading-edge separation vortex over a delta wing at high angle of attack by Fujii and Kutler,[10] the simulation of a tip vortex off a low-aspect-ratio wing at a transonic speed by Mansour,[11] and the transonic wing solutions of Agarwal and Deese,[12] Vadyak,[13] Obayashi and Fujii,[14] and Holst et al.[15] are a few examples of calculations of viscous three-dimensional flows.

In the present study, a computer program called transonic Navier-Stokes (TNS), which was developed by Holst et al.,[15] is used to compute the viscous flowfield around a low-aspect-ratio wing. The TNS program was chosen because of its speed, accuracy, and efficiency. Its convergence characteristics were given by Flores,[16] and its data management scheme was described by Holst et al.[17]

The particular geometry of interest is the so-called WING C, which is a generic advanced technology wing. It has an aspect ratio of 2.6, a twist angle of 8.17 deg, a taper ratio of 0.3, and a leading-edge sweep of 45 deg. A series of WING C flow cases are solved in the Mach number range of 0.70–0.90 at an angle of attack of 5 deg, with the Reynolds number based on the mean aerodynamic chord of 6.8×10^6.

Numerical Method

Zonal Approach

Most of the Navier-Stokes solutions mentioned in the previous section generally utilized relatively coarse grids and required large amounts of computer time even on the latest supercomputers. One method that could improve the situation is the use of zonal grids, which is the methodology followed in the TNS program. In this approach, zonal grid generation starts with the generation of a global single-zone grid that includes the entire flowfield. This grid contains no fine-mesh regions to capture viscous effects and has an H-mesh topology in both the spanwise and chordwise directions. In this study, the global grid was generated by the elliptic solver approach of Sorenson and Steger.[18]

Presented as Paper 86-0508 at the AIAA 24th Aerospace Sciences Meeting, Reno, NV, Jan. 6-9, 1986; received July 22, 1986; revision received Nov. 24, 1986.

*Research Scientist. Member AIAA.
†Chief, Applied Computational Fluids Branch. Associate Fellow AIAA.
‡Associate Professor, Department of Aeronautics and Astronautics.
§Research Scientist, Applied Computational Fluids Branch. Member AIAA.

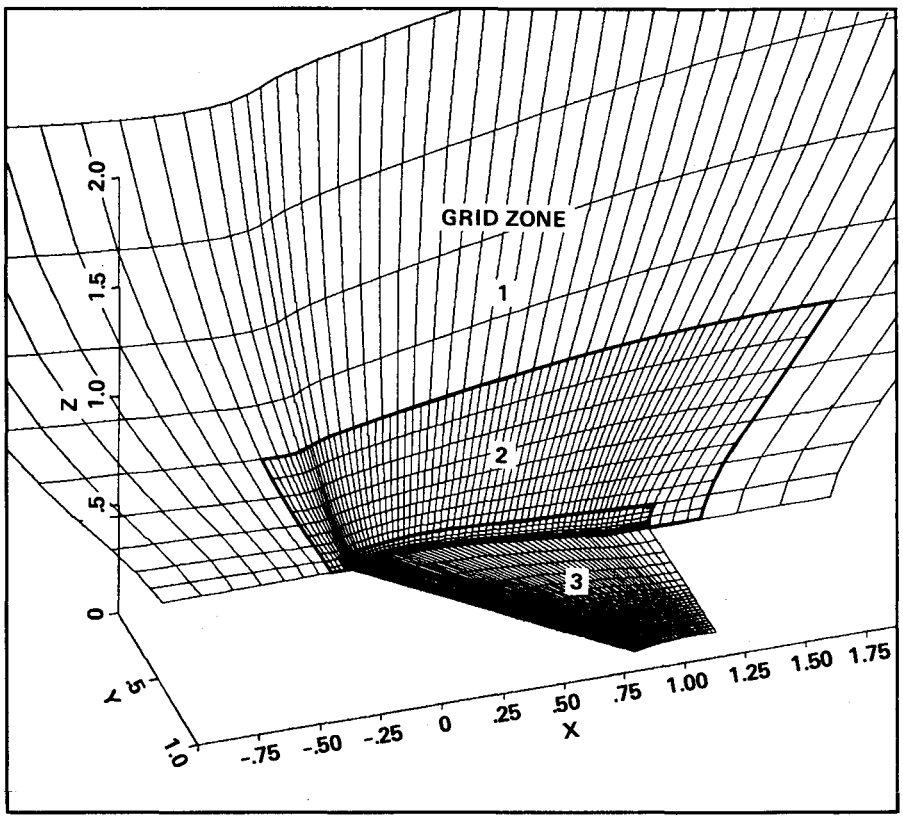

Fig. 1 Perspective view of embedded grid with upper symmetry plane ($y=0$, $z\geq 0$) and wing surface highlighted.

Once the base grid is generated, it is divided into zones utilizing a "zoning" algorithm. In the present TNS code, an isolated wing grid is configured with four zones. A perspective view of a typical grid, which shows different zones in the vicinity of the wing, is presented in Fig. 1. The first grid zone (grid 1) is the coarse base grid itself with a small three-dimensional domain left open. The second grid zone (grid 2) fills this open domain with a small overlap region in common with grid 1 and also has another small three-dimensional domain left open for the third and fourth grids. Grid 2 contains twice as many grid points in each spatial direction as the original base grid.

The final two grid zones (grids 3 and 4) occupy the space that is left open by the block of points removed from grid 2, again with a small region of overlap included. Grids 3 and 4 contain the same number of points in both the spanwise and chordwise directions as grid 2. However, they are designed to capture the viscous effects on the wing and the grid points in the normal direction are highly clustered. Note that only grids 1-3 are shown in Fig. 1. The total number of grid points used in the zonal grid of Fig. 1 is 165,321. The individual grid point breakdown for each zone is as follows: grid 1, $63\times26\times25=40{,}950$; grid 2, $69\times29\times21=42{,}021$; grid 3, $61\times27\times25=41{,}175$, and grid 4, $61\times27\times25=41{,}175$, where the individual numbers in each zone designate the number of grid points in the streamwise, spanwise, and normal directions, respectively.

Governing Equations and Numerical Algorithm

The equations solved in this study are the Euler and Reynolds-averaged Navier-Stokes equations written in strong conservation form. The Reynolds-averaged equations are simplified by using the standard thin-layer approximation[19] for the viscous terms and are used to solve the flowfield in the vicinity of the wing where viscous effects are important. The Euler equations are solved in regions away from the wing where viscous forces are not significant. The Pulliam-Steger ARC3D computer code[20] is used as the main integration routine.

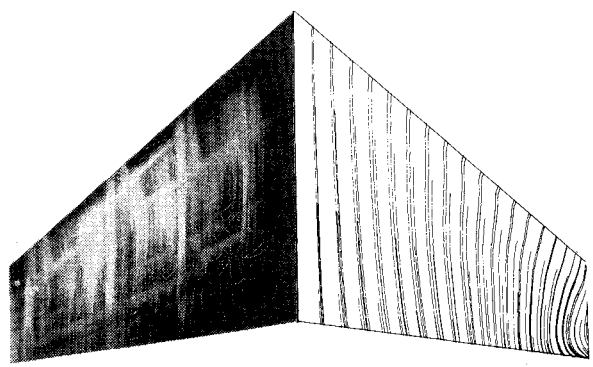

Fig. 2 Experimental oil-flow picture (from Ref. 30) and computed upper surface skin-friction lines for WING C: $M_\infty=0.82$, $\alpha=5$ deg, $Re_{\text{m.a.c.}}=6.8\times10^6$.

The numerical algorithm associated with the ARC3D computer code is an ADI algorithm developed by Pulliam and Chaussee[21] that requires the solution of scalar pentadiagonal matrices. This scheme uses the standard second-order-accurate central differencing of the governing equations, fourth-difference implicit and explicit artificial dissipation terms on the left- and right-hand sides of the algorithm, and a variable time step scaled by the Jacobian. The turbulence model used in the TNS computer program is the Baldwin-Lomax algebraic model[19] for high Reynolds number turbulent flows. Additional details of the present work can be found in Kaynak et al.[22]

Overview of Separated Flows

The character of a flow near a surface, to a large extent, can be inferred from the surface pattern or "skin-friction lines," which are the lines everywhere parallel to the wall shear stress vectors. As Lighthill has stated,[23] the pattern of skin-friction lines can often be approximately determined by

the experimental oil flow technique. Although the definition of separation and reattachment is well established in two-dimensional flows by the existence of a reverse flow, a straightforward extrapolation of two-dimensional concepts to three-dimensional flows is not possible. In three dimensions, the meaning of the term "reverse" becomes ambiguous. Our present understanding of three-dimensional separation stems essentially from flow visualization experiments. If, for instance, a surface oil flow technique is used, Tobak and Peake[24] state that the convergence of oil streaks onto a particular line is a *necessary* condition for three-dimensional separation. But whether this is also a *sufficient* condition is a topic of current debate.

Skin-friction lines are defined as the integral curves of the wall shear stress vector exerted by the fluid on the wall. There is only one skin-friction line through each point on a surface, except for a point of separation or reattachment, where the wall shear stress vanishes. These points are the singular points of the differential equations governing the topography of the skin-friction lines. Such singular points are classified as nodes, saddles, and foci, depending on the mathematical properties of the governing differential equations.[25] The total number of singular points for a possible pattern on a smooth surface is subject to a topological law. Mathematicians have shown that the number of nodal points must exceed the number of saddle points by two.[25] Also, it has been shown that a combination of two saddle points in which a streamline emanating from one point yields to another is not allowed because of stability considerations.[26]

Computation of WING C Flowfields

WING C Design and Testing

In recent years, there have been significant efforts to compute flowfields around wings in the transonic regime. Consequently, it is important to assess the accuracy of these computations by comparing them with reliable experimental data. In particular, an advanced technology wing called WING C was tested in two different facilities by Hinson and Burdges[27] and Keener[30] in a cooperative effort. The WING C geometry is composed of supercritical airfoils with relatively thick sections that produce moderate aft loading, relatively weak shock waves, and a mild pressure recovery. The design conditions selected were a Mach number of 0.85 and a lift coefficient of approximately 0.5 at an angle of attack of 5 deg. The mild shock wave was accomplished by limiting the leading-edge normal Mach numbers in the vicinity of the leading edge to a maximum of 1.2. This value is commonly accepted as the upper limit for preventing shock-induced flow separation in the wing design.

A small-scale 0.261 m semispan model of WING C was tested by Hinson and Burdges.[27] The test Reynolds number based on the mean aerodynamic chord was 10×10^6. Surface pressures were measured both on the wing and on wind tunnel walls for comparison with calculations. The small-scale data of Ref. 27 are compared with several three-dimensional transonic inviscid potential codes in Refs. 28 and 29. The experimental facility is a blowdown wind tunnel. The top and sidewalls of the three-dimensional test section have a variable porosity capacity of up to 10%. The model blockage ratio is

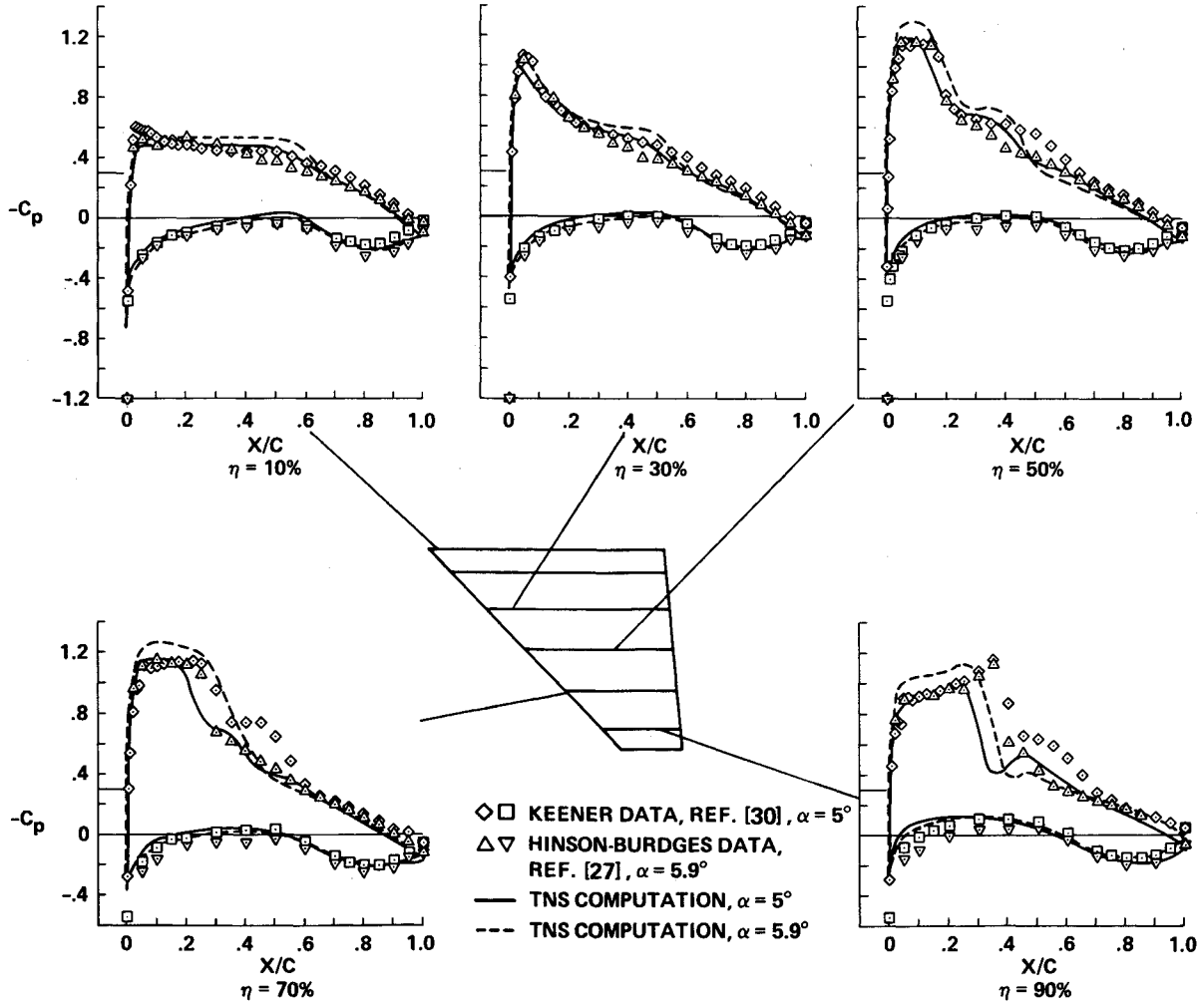

Fig. 3 Comparison of experimental and computed pressure coefficients for WING C: $M_\infty = 0.85$, $Re_{\text{m.a.c.}} = 6.8\times10^6$.

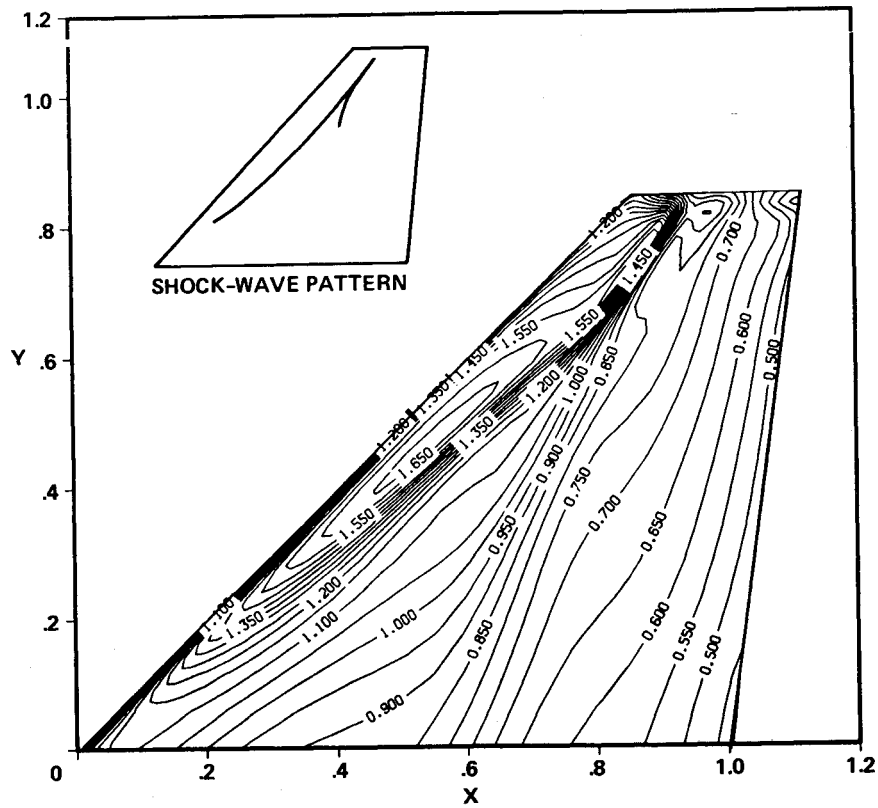

Fig. 4 Mach number contours on the upper surface of WING C: $M_\infty = 0.85$, $\alpha = 5$ deg, $Re_{\text{m.a.c.}} = 6.8 \times 10^6$.

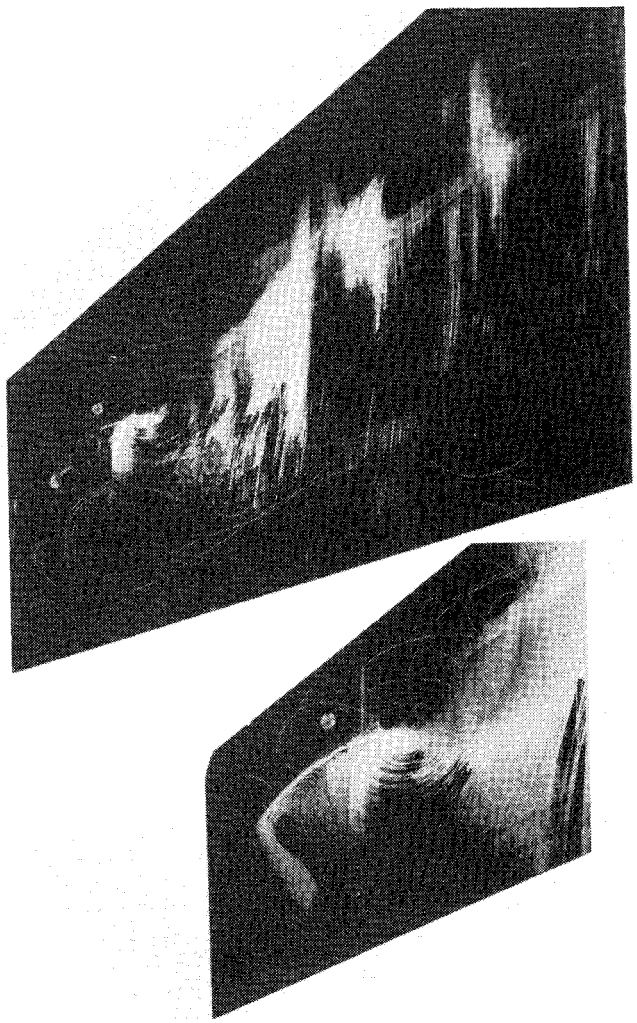

Fig. 5 Experimental oil flow picture (from Ref. 30) and an expanded view of the counterrotating vortices for WING C: $M_\infty = 0.85$, $\alpha = 5$ deg, $Re_{\text{m.a.c.}} = 6.8 \times 10^6$.

about 1%. Most of the wind tunnel testing was conducted at a fixed-wall porosity of 4% for minimum wall interference effects. The influence of the wind tunnel walls on the test data was explored and it was found that a Mach number correction of $\Delta M = -0.005$ was necessary. An angle-of-attack correction of $\Delta\alpha = 0.9$ deg was also needed in the experiments to match the computations. The method of matching leading-edge pressures was used to select an experimental angle of attack of 5.9 deg, for which the experimental and computed (using a potential flow code with $\alpha = 5$ deg) leading-edge pressures agreed. Transition strips were located at a fixed distance from the leading edge equal to 5% of the mean aerodynamic chord on both the upper and lower surfaces of the wing.

A series of tests with the WING C was also performed by Keener[30] as a part of the cooperative effort. A large-scale 0.90 m semispan model was tested in a (1.8×1.8 m) wind tunnel. Model blockage ratio in the test section was 1.3% at zero angle of attack. Surface pressure measurements and oil flow studies were made at the design angle of attack of 5 deg over a Mach number range of 0.25–0.96 and a Reynolds number range of $3.4\text{–}10 \times 10^6$. No Reynolds number effect on the results was reported. The lift interference from the tunnel walls was reported to be small. This is because the leading-edge pressures of the experiment and computations in the correlations happened to agree with each other at the design angle of attack by 5 deg. Transition strips were installed at 4.5% of chord.

Attached Flow Cases

The first set of WING C flow computations using the TNS program to be discussed will be attached flow cases. These cases are included to demonstrate the two-dimensional nature of the flow in the attached flow regime. This two-dimensional flow aspect was part of the design goal undertaken by the WING C design project. Attached flow calculations were obtained for two supercritical cases: $M_\infty = 0.70$ and 0.82 at $\alpha = 5$ deg, and $Re = 6.8 \times 10^6$. In all these and subsequent computations, the Reynolds number is based on the mean aerodynamic chord (m.a.c.) of the WING C and the turbulent flow calculations are started at the leading edge

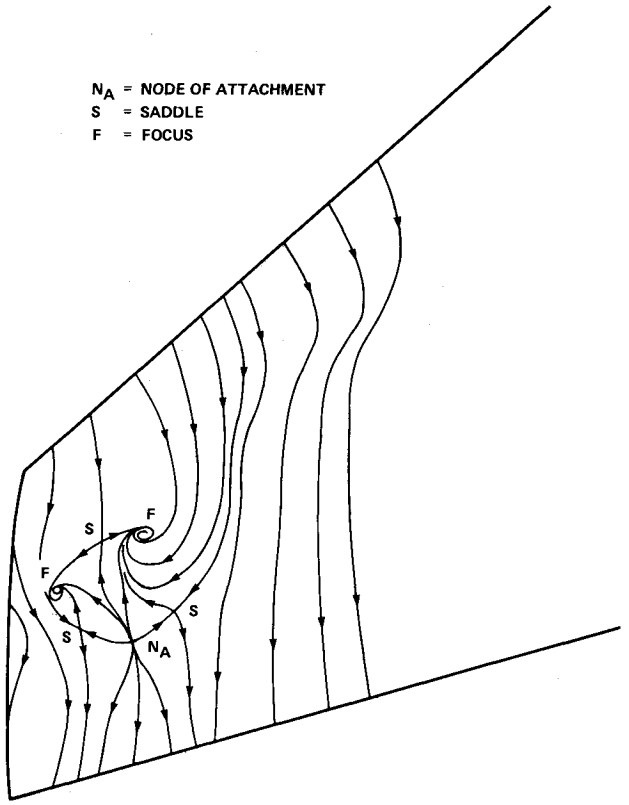

Fig. 6 "Postulated" skin-friction lines for the WING C case shown in Fig. 5 ($M_\infty = 0.85$).

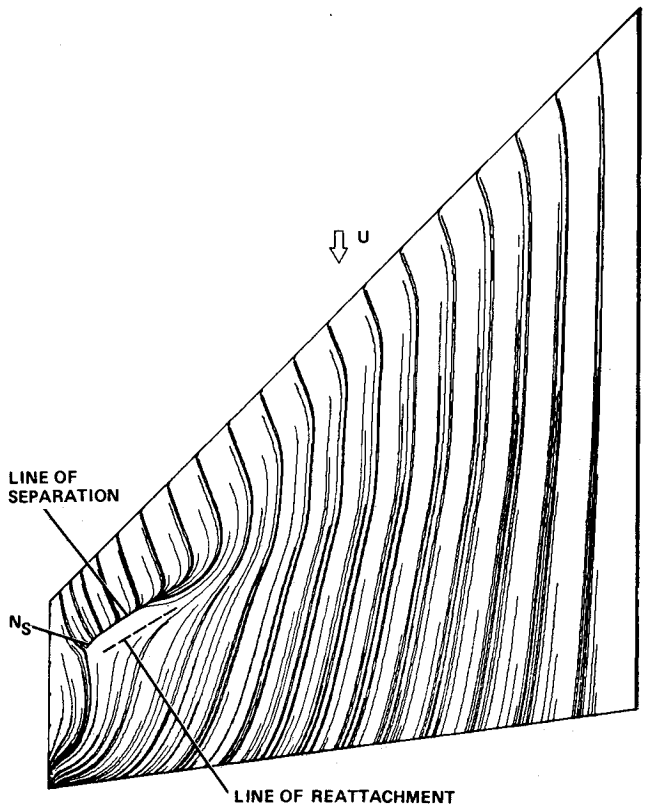

Fig. 7 Computed skin-friction lines for WING C upper surface: $M_\infty = 0.85$, $\alpha = 5.9$ deg, $Re_{\text{m.a.c.}} = 6.8 \times 10^6$.

without any transition model. The general features of these two cases are similar as far as the pressure and skin-friction fields are concerned. Therefore, only the latter case with $M_\infty = 0.82$, $\alpha = 5$ deg, and $Re = 6.8 \times 10^6$ will be presented.

Figure 2 shows an experimental oil flow photograph on the left and the computed skin-friction lines on the right. In the oil flow picture, only a weak design shock wave is observed, indicated by a slight S-shape in the oil streak lines that lie in the outboard section of the wing between approximately 15 and 25% of chord. This shock wave is not strong enough to separate the boundary layer, contrary to the earlier computations by Mansour.[11] The flow is almost two-dimensional, with flow deflection angles less than 10 deg, except near the leading edge. The agreement between computation and experiment is good for this case. Also, the correlation between the experimental and the computational sectional pressure coefficients is quite encouraging. It is not given here because of space limitations, but the interested reader is referred to Ref. 22.

Separated Flow Cases

In this section, a series of transonic separated flow computations will be presented. The methodology of studying these flows will be from three points of view: 1) the actual phenomena, i.e., the experimental flow pictures; 2) the "conceptualization" or the "postulation" of these pictures in light of topological laws and rules; and 3) the computations. In any kind of interpretation, these three topics must support each other to provide a plausible explanation. The surface phenomenon is very important because the three-dimensional flowfield above the surface depends on the surface flow. For instance, three-dimensional stream surfaces emerge from the separation lines, whereas rolled-up vortex sheets emanate from spiral separation nodes, i.e., the foci. However, the three-dimensional separation phenomenon is very complex and a given surface pattern can produce many three-dimensional flow patterns depending upon interpretation. Dallman[31] explains with examples that there is no unique relationship between the pattern of wall streamlines and the flowfield above the wall. He adds that topologically different flowfields may exhibit the same oil flow picture.

The first separated flow case consists of the WING C design conditions $M_\infty = 0.85$, $\alpha = 5$ deg, and $Re = 6.8 \times 10^6$. These conditions were intended to result in attached flow with a mild shock wave and a mild pressure recovery. But, for reasons discussed in Ref. 30, these conditions produced a "local" (as called by its author) flow separation. In this work, the adjectives such as "local" vs "global" or "open" vs "closed" will be avoided because of the current debate on the definition of different types of three-dimensional separations. However, the interested reader may refer to Ref. 24 for particulars.

The calculated pressure coefficient distributions are compared with experimental data in Fig. 3. Note that in this figure the angle of attack for the Keener data[30] is 5 deg, whereas for the Hinson and Burdges data,[27] it is 5.9 deg in accordance with their accounting for wall effects. Consequently, computations were obtained for these two angles of attack ($\alpha = 5$ and 5.9 deg) at $M_\infty = 0.85$ and $Re = 6.8 \times 10^6$. The computation with $\alpha = 5$ deg agrees with the two experiments better in terms of matching leading-edge pressures. On the other hand, the results with $\alpha = 5.9$ deg seem to agree better with experiments in terms of shock position and lower surface pressures. Particularly, at the 70 and 90% spanwise stations, there is a marked improvement in the shock location, which is the key to obtaining a separated flow. This point will be clarified later in conjunction with Fig. 7. Note that the differences between the two computations and the two experiments are generally of the same order of magnitude. The experimental differences may be explained by considering the uncertainties in the measurements of the Mach number and the angle of attack and the assessment of the wall interference effects associated with the experiments. Possible distortions in the wing geometries caused by

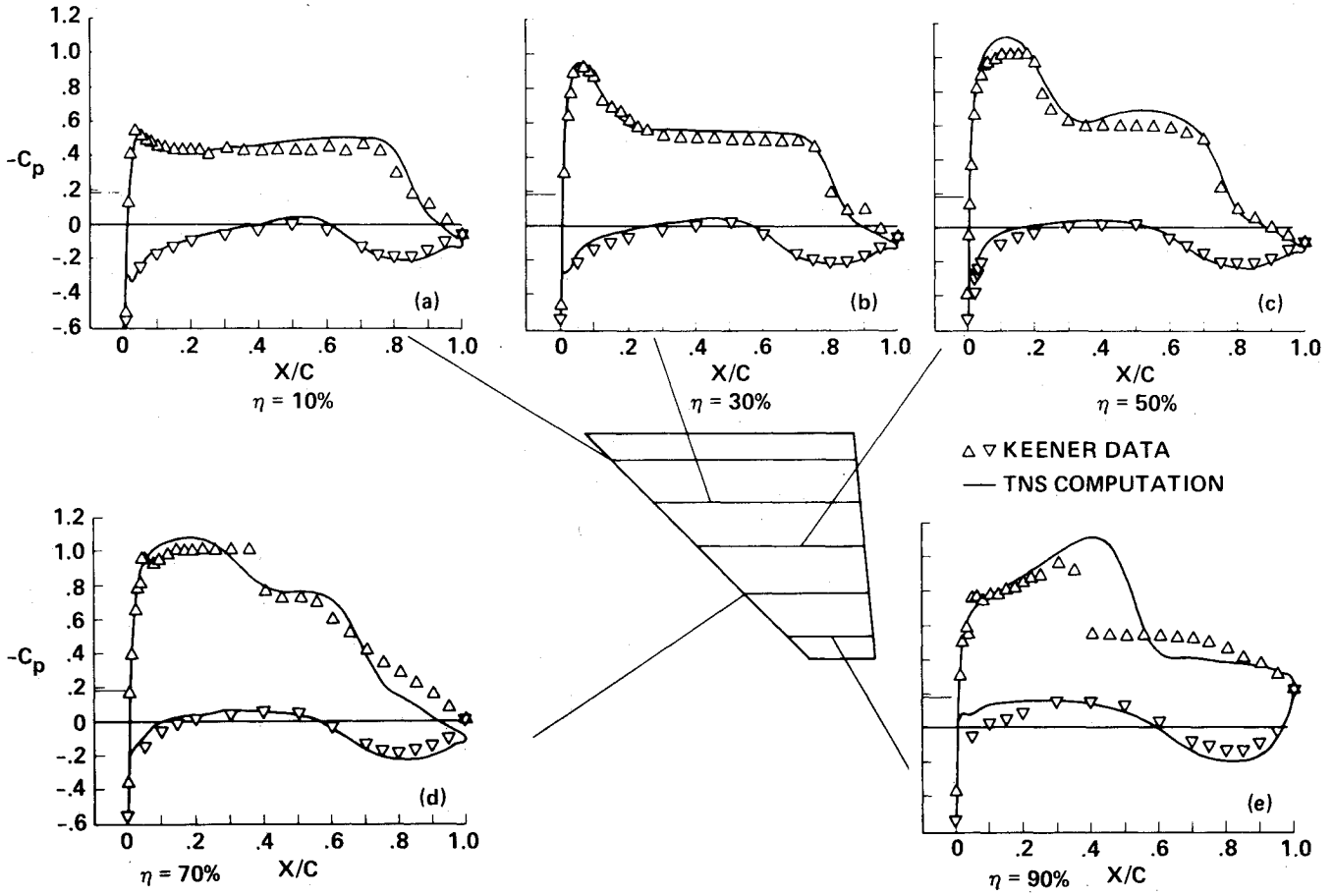

Fig. 8 Comparison of experimental and computed pressure coefficients for WING C: $M_\infty = 0.90$, $\alpha = 5$ deg, $Re_{\text{m.a.c.}} = 6.8 \times 10^6$.

aerodynamic forces and moments during the experiments might also have affected the measurements. On the other hand, the numerical simulation has its own difficulties primarily associated with the coarse grid near the tip and the inadequate turbulence model. However, the overall comparison is encouraging, considering the above-mentioned uncertainties. Figure 4 shows the wing planform Mach number contours plotted at a location above the upper wing surface, which display the well-known transonic lambda shock wave pattern.

The experimental oil flow picture for the same case is presented in Fig. 5. Figure 6 shows the *postulated* skin-friction field. A separation line caused by the swept shock wave emanates from a saddle point with two counter-rotating vortices on either side. The postulated skin-friction map also features two other saddle points and one nodal point of attachment. In three-dimensional separation, it is not possible to define a closed separation or "bubble" as in two dimensions. Here the separation zone is largely fed by the vortical flow on the inboard side of the saddle point of separation. The tip flow is highly curved inboard toward the separation zone, but does not enter the zone. Also, some streamlines are entrapped by the inboard vortex, whereas others pass by the separation region without being trapped. The flow is almost two-dimensional outside the separation zone.

The computed skin-friction lines for this case are presented in Fig. 7. First of all, the calculation with $\alpha = 5$ deg did not display a separated flow, because, as will be remembered from Fig. 3, the shock wave strength and location at the 70 and 90% span stations were not well predicted, so that the shock was not adequate to separate the flow. Therefore, $\alpha = 5.9$ deg was used instead of 5 deg in Fig. 7. It was this angle-of-attack correction that moved the shock wave downstream in better agreement with the experiment and

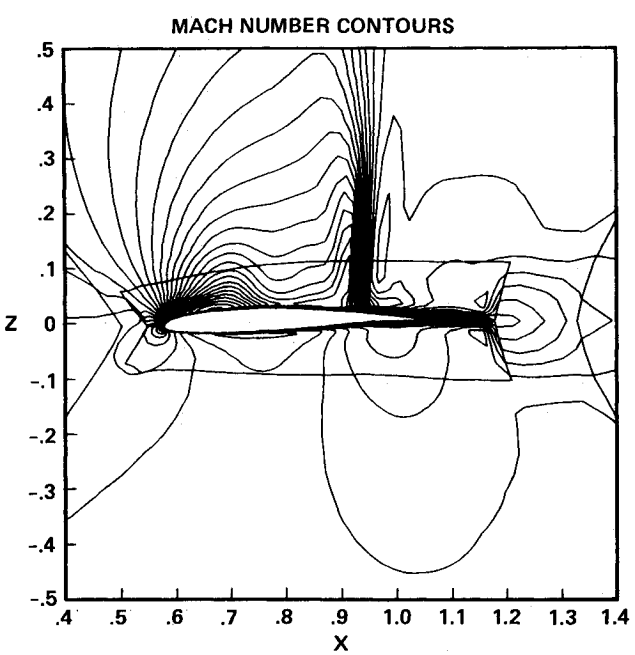

Fig. 9 Cross-sectional Mach number contours for WING C at $2y/b = 0.77$: $M_\infty = 0.90$, $\alpha = 5$ deg, $Re_{\text{m.a.c.}} = 6.8 \times 10^6$.

caused the flow to separate. As a result, the global features of the experiment are predicted well. The location and size of the separation line, the streamlines being trapped by the vortex-like formation inboard of the separation line, the curvature of the tip streamlines, and the almost two-dimensional flow outside the separation zone are all accurately predicted. However, the critical points of the skin-

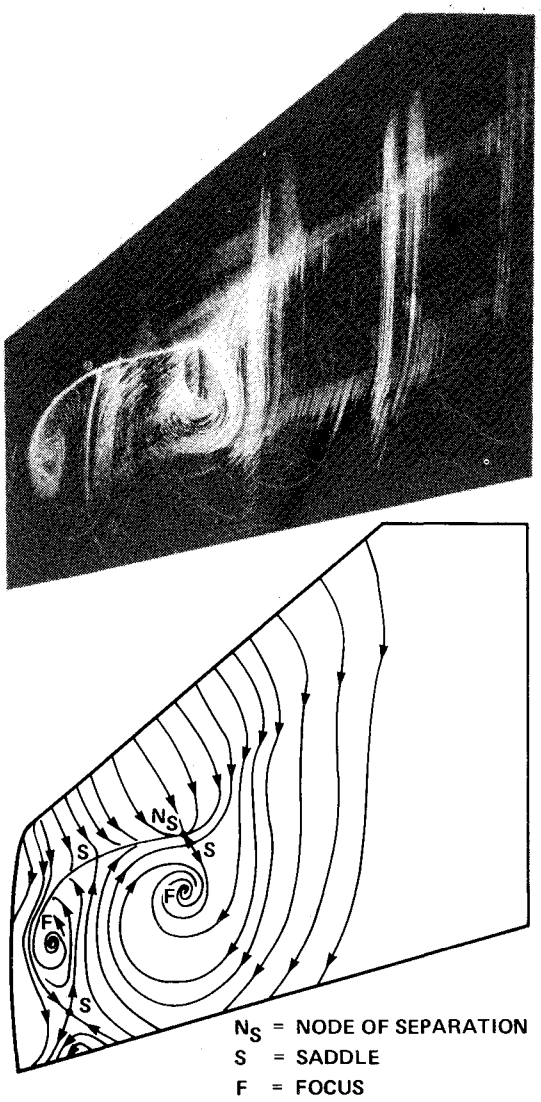

Fig. 10 Experimental oil-flow picture (from Ref. 30) and "postulated" skin-friction lines for WING C: $M_\infty = 0.90$, $\alpha = 5$ deg, $Re_{\text{m.a.c.}} = 6.8 \times 10^6$.

friction map were not well reproduced, but a nodal point N_s along the line of separation and near the tip is predicted. Overall, the simulation is encouraging. Although not done explicitly for WING C, it has been shown[32] for a similar case that a computational critical point map similar to the experimental one can be produced. By refining the grid and using a better turbulence model, the weak vortical flow inboard of the line of separation in the present computation could be modified to produce a vortex similar to the one in Fig. 5. Since there is already a nodal point on the other side of the line of separation, the emergence of a saddle point between them is inevitable as dictated by topological laws.[23] This is exactly the main feature of the experimental photograph in Fig. 5 as interpreted in Fig. 6; a line of separation emanating from a saddle point with two counterrotating vortices on each side.

The second separated case associated with WING C consists of a flow at off-design conditions: $M_\infty = 0.90$, $\alpha = 5$ deg, and $Re = 6.8 \times 10^6$. The computed and experimental pressure coefficient distributions are compared in Fig. 8. The leading edge and aft shock waves are stronger than those of the previous case and the aft shock wave is further downstream. This is a consequence of the increased freestream Mach number. Despite the discrepancy in shock location at the tip, the overall agreement between experiment and computation for this difficult case is encouraging. The disagreement at the tip is probably caused by coarse grid effects and the other

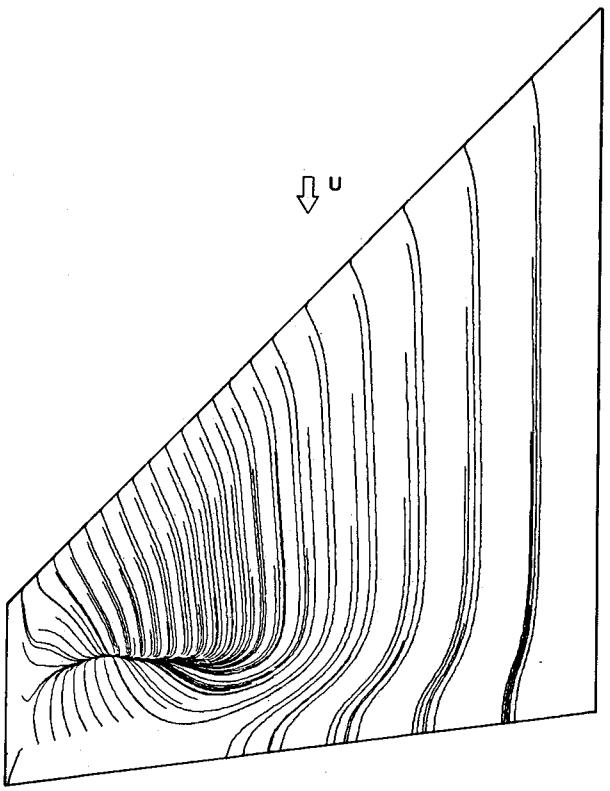

Fig. 11 Computed skin-friction lines for WING C upper surface: $M_\infty = 0.90$, $\alpha = 5.0$ deg, $Re_{\text{m.a.c.}} = 6.8 \times 10^6$.

reasons already discussed in the previous case ($M_\infty = 0.85$). The Mach number contours in the streamwise cross-sectional plane at $\eta = 0.77\%$ of semispan is shown in Fig. 9. The zonal boundaries are also shown in this plot. Note the smoothness with which the shock wave crosses the zonal interface boundary. This indicates that the communication between the zones is implemented in a conservative manner. In addition, most of the other contours cross the zonal interface boundaries in a smooth and continuous fashion. Downstream in the wake, where the fine grid used to capture viscous effects interfaces with a relatively coarse grid (see Fig. 1), the wake abruptly stops. This aspect of the solution exists because the coarse inviscid grid cannot retain the sharp wake velocity gradient.

The surface oil flow photograph and the present *postulation* of the skin-friction lines for this case are presented in Fig. 10. When the Mach number is increased from 0.85 to 0.90, the flow separation that existed over the outer 30% of the wing moves slightly downstream and grows significantly in size. The counterrotating vortices that emerged in the previous case grow substantially, and the larger vortex inboard of the separation line extends as far as the trailing edge. A line of separation emerges from the saddle point of separation. There is one focus on the tip side and a node of separation on the inboard side of this line. Another saddle point exists near this node of separation. This saddle point lies between the node and the second, larger focus. There exists another saddle point near the trailing edge. The inboard vortex is strong and provides a mechanism to feed fluid into the separation zone by entrapping the streamlines coming from the inboard side of the separation zone. The flow between the separation zone and the symmetry plane is again almost two-dimensional, except for a streamline deflection caused by the inboard vortex.

The computed skin-friction lines for the same case ($M_\infty = 0.90$) are presented in Fig. 11. As observed, the agreement between the computed skin-friction lines and the experiment in Fig. 10 is rather poor, mainly because of the coarse grid effects and inadequate turbulence modeling. A

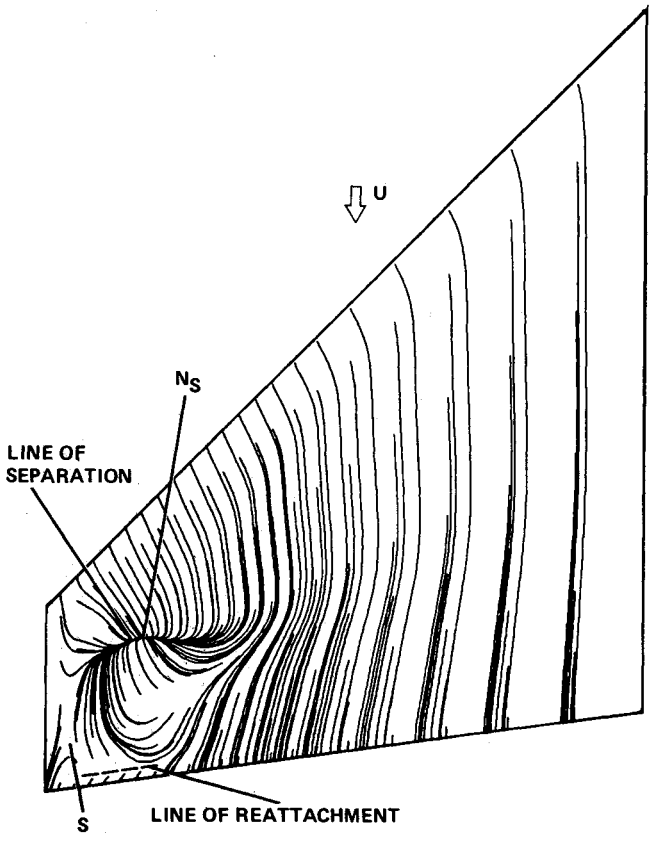

Fig. 12 Computed skin-friction lines for WING C upper surface: $M_\infty = 0.88$, $\alpha = 5.0$ deg, $Re_{m.a.c.} = 6.8 \times 10^6$.

weak swirling motion is exhibited in the computation on the inboard side of the separation zone, yet the smaller vortex near the tip is nonexistent. Because of the coarseness of the present grid near the tip, this vortex is probably not resolvable. The disagreement occurs close to the tip, where the computation does not capture the shock location well. It is this poor shock location that moves the separation line too close to the trailing edge and causes the disagreement between experiment and computation. In an attempt to better align the computed line of separation with that of the experiment, this case was recalculated at a slightly lower Mach number. It was found that when the Mach number was reduced slightly, to 0.88, significant changes were observed that were in closer agreement with the $M_\infty = 0.90$ experiment.

The computed skin-friction lines for this slightly lower Mach number are shown in Fig. 12. This flow pattern is indeed more descriptive of the experimental oil flow at $M_\infty = 0.90$. The line of separation moves forward, in better agreement with the experiment, and there is substantially stronger vortical flow in the area of the inboard vortex. The node of separation in the experiment was captured. The saddle point that lies near the trailing edge of the wing in the experiment was also captured. However, the vortex close to the tip has not been resolved. Had this vortex been resolved, the emergence of a saddle point between this vortex and the node would have been automatic, according to the continuity equation.[23] The computation also predicts a reattachment line at the trailing edge near the tip, although this does not exist in the experiment. To recapitulate, although quantitative details are not accurately reproduced, many qualitative details are. The location and extent of separation are in reasonable agreement with experiment, as is the pressure distribution. The onset of vortex formation evident in the experiment is also present in the computation. It should be re-emphasized that experimental uncertainties associated with wind tunnel wall interference, angle-of-attack measurement, freestream Mach number measurement, etc., must be considered in evaluating the computational/experimental correlations.

Conclusions

Transonic flowfields around the so-called WING C configuration have been simulated using a zonal-type viscous/inviscid algorithm. The flowfield around the wing was divided into four zones and concurrently solved using appropriate equation sets as the flow physics suggests. Grid points in zones immediately adjacent to the wing were finely clustered and the flow here was solved using the Reynolds-averaged Navier Stokes equations in the standard "thin-layer" form to simulate viscous effects. Grid zones away from the wing had less finely clustered points and the flow in these regions was solved with the Euler equations to capture inviscid-rotational effects.

A series of WING C flow cases was calculated in the transonic regime with Mach numbers of 0.70–0.90. These cases include attached and separated flows. All cases produced good agreement with experiment in terms of the pressure field. Also, for the first time, an encouraging correlation between a computed separated surface flow ($M_\infty = 0.85$) and an experimental oil flow photograph was obtained. The separation pattern of another case ($M_\infty = 0.88$) also showed a qualitative agreement with the experiment.

Acknowledgment

The first author would like to acknowledge support from the NASA Ames Research Center through Contract NCA2-OR745-309 and from the Scientific and Technical Research Council of Turkey through a fellowship.

References

[1]Mehta, U. and Lomax, H., "Reynolds Averaged Navier-Stokes Computations of Transonic Flows, The State-of-the-Art," *AIAA Progress in Astronautics and Aeronautics: Transonic Aerodynamics,* Vol. 81, edited by D. Nixon, AIAA, New York, 1982, pp. 297–375.

[2]Levin, D. and Katz, J., "Vortex-Lattice Method for the Calculation of the Nonsteady Separated Flows over Delta Wings," *Journal of Aircraft,* Vol. 18, Dec. 1981, pp. 1032–1037.

[3]Johnson, F. T., Tinocco, E. N., Lu, P., and Epton, M. A., "Recent Advances in the Solution of Three-Dimensional Flows over Wings with Leading Edge Separation," AIAA Paper 79-0282, Jan. 1979.

[4]Ericsson, L.E. and Rizzi, A., "Computation of Vortex Flow around Wings Using Euler Equations," *Proceedings of Fourth GAMM Conference on Numerical Methods in Fluid Methods,* Vieweg-Verlag, Paris, 1981.

[5]Hitzel, S. M. and Schmidt, W., "Slender Wings with Leading-Edge Vortex Separation—A Challenge for Panel-Methods and Euler-Codes," AIAA Paper 83-0562, Jan. 1983.

[6]Krause, E., Shi, X. G., and Hartwich, P. W., "Computation of Leading-Edge Vortices," AIAA Paper 83-1907, July 1983.

[7]Raj, P. and Sikore, J. S., "Free-Vortex Flows: Recent Encounters with an Euler Code," AIAA Paper 84-0135, Jan. 1984.

[8]Steger, J. L. and Van Dalsem, W. R., "Developments in the Simulation of Separated Flows Using Finite Difference Methods," *Third Symposium on Numerical and Physical Aspects of Aerodynamic Flows,* Long Beach, CA, Jan. 1985.

[9]Vigneron, Y. C., Rakich, J. V., and Tannehill, J. C., "Calculation of Supersonic Viscous Flow over Delta Wings with Sharp Subsonic Leading Edges," AIAA Paper 78-1137, July 1978.

[10]Fujii, K. and Kutler, P., "Numerical Simulation of the Viscous Flow Fields Over Three-Dimensional Complicated Geometries," AIAA Paper 84-1550, June 1984.

[11]Mansour, N. N., "Numerical Simulation of the Tip Vortex Off a Low-Aspect Ratio Wing at Transonic Speed," AIAA Paper 84-0522, Jan. 1984.

[12]Agarwal, R. K. and Deese, J. E., "Computation of Transonic Viscous Airfoil, Inlet, and Wing Flowfields," MDRL Rept. 84-29, June 1984 (also AIAA Paper 84-1551, June 1984).

[13]Vadyak, J., "Simulation of Wing, Fuselage, and Wing/Fuselage Flowfields Using a 3D Euler/Navier-Stokes Algorithm," AIAA Paper 85-1693, July 1985.

[14]Obayashi, S. and Fujii, K., "Computation of Three-Dimensional Viscous Transonic Flows with the LU Factored Scheme," AIAA Paper 85-1510, July 1985.

[15]Holst, T. L., Kaynak, U., Gundy, K. L., Thomas, S. D., Flores, J., and Chaderjian, N., "Numerical Solution of Transonic Wing Flows Using an Euler/Navier-Stokes Zonal Approach," *Journal of Aircraft*, Vol. 24, Jan. 1987, pp. 17-24.

[16]Flores, J., "Convergence Acceleration for a Three-Dimensional Euler/Navier Stokes Zonal Approach," AIAA Paper 85-1495, July 1985.

[17]Holst, T. L., Thomas, S. D., Kaynak, U., Gundy, K. L., Flores, J., and Chaderjian, N. M., "Computational Aspects of Zonal Algorithms for Solving the Compressible Navier-Stokes Equations in Three-Dimensions," *International Symposium on Computational Fluid Dynamics,* Tokyo, Sept. 9-12, 1985.

[18]Sorenson, R. L. and Steger, J. L., "Grid Generation in Three Dimensions by Poisson Equations with Control of Cell Size and Skewness at Boundary Surfaces," *Advances in Grid Generation—FED,* Vol. 5, edited by K. N. Ghia, 1983.

[19]Baldwin, B. S. and Lomax, H., "Thin-Layer Approximation and Algebraic Model for Separated Turbulent Flows," AIAA Paper 78-257, Jan. 1978.

[20]Pulliam, T. H., "Euler and Thin-Layer Navier-Stokes Codes: ARC2D and ARC3D," *Notes for the Computational Fluid Dynamics Users' Workshop,* University of Tennessee Space Institute, Tullahoma, March 1984.

[21]Pulliam, T. H. and Chaussee, D. S., "A Diagonal Form of an Implicit Approximate-Factorization Algorithm," *Journal of Computational Physics,* Vol. 39, Feb. 1981, pp. 347-363.

[22]Kaynak, Ü., Holst, T. L., Cantwell, B. J., and Sorenson, R. L., "Numerical Simulation of Transonic Separated Flows over Low-Aspect Ratio Wings," AIAA Paper 86-0508, Jan. 1986.

[23]Lighthill, M. J., "Attachment and Separation in Three-Dimensional Flow," *Laminar Boundary Layers,* edited by L. Rosenhead, Oxford University Press, London, 1963, pp. 72-82.

[24]Tobak, M. and Peake, D. J., "Topological Structures of Three-Dimensional Separated Flows," AIAA Paper 81-1260, June 1981.

[25]Kaplan, W., *Ordinary Differential Equations,* Addison-Wesley, London, 1958.

[26]Andronov, A. A., Leontovich, E. A., Gordon, I. I., and Maier, A. G., "Theory of Bifurcations of Dynamic Systems on a Plane," NASA TT F-556, 1971.

[27]Hinson, B. L. and Burdges, K. P., "Acquisition and Application of Transonic Wing and Far-Field Test Data for Three-Dimensional Computational Method Evaluation," Vol. II, Appendix B, AFOSR-TR-80-0422, 1980.

[28]Hinson, B. L. and Burdges, K. P., "Acquisition and Application of Transonic Wing and Far-Field Test Data for Three-Dimensional Computational Method Evaluation," AFOSR-TR-80-0421, 1980.

[29]Hinson, B. L. and Burdges, K. P., "An evaluation of Three-Dimensional Transonic Codes Using New Correlation Test Data," AIAA Paper 80-0003, 1980.

[30]Keener, E. R., "Computational-Experimental Pressure Distributions on a Transonic, Low-Aspect-Ratio Wing," AIAA Paper 84-2092, Aug. 1984.

[31]Dallmann, U., "Topological Structures of Three-Dimensional Vortex Flow Separation," AIAA Paper 83-1735, July 1983.

[32]Kaynak, Ü., "Computation of Transonic Separated Wing Flows Using an Euler/Navier-Stokes Zonal Approach," Ph.D. Thesis, Dept. of Aeronautics and Astronautics, Stanford University, Stanford, CA, Dec. 1985.